Journal of Nanobiotechnology

RESEARCH

Open Access

Catalase-encapsulated matrix metalloproteinase-9 responsive nanogels for modulation of inflammatory response and treatment of neutrophilic asthma

Xiaoping Guo[1,4], Xu Zuo[1], Wenxue Zheng[1], Dan Zhao[2], Chao Dong[3], Zheng Zou[2], Yuanyuan Shen[2], Caina Xu[1,4*], Chaoliang He[2*] and Fang Wang[1,4*]

Abstract

Asthma is a chronic disease with typical pathological features such as airflow limitation, airway inflammation and remodeling. Of these, neutrophilic asthma is considered to be the more severe and corticosteroid-resistant subtype of asthma. Increasing evidence suggests that patients with neutrophilic asthma often accompany with dysbiosis of the internal microbiota, where the increased abundance of non-typeable Haemophilus influenzae (NTHi) is closely related to the neutrophilic asthma phenotype. Furthermore, emerging evidence suggests that reactive oxygen species (ROS) are pivotal in the pathogenesis of neutrophilic asthma. In this study, matrix metalloproteinase-9 (MMP-9)-responsive, catalase-loaded nanogels (M-CAT-NGs) were synthesized, which was composed of MMP-9-sensitive peptide (VPMS), arginine-grafted chitosan and maleimide (CS-Arg-Mal), catalase (CAT), sodium citrate (SC) and ε-poly(L-lysine) (ε-PLL). The M-CAT-NGs showed potent antimicrobial effects and exerted excellent therapeutic effects in the presence of MMP-9 by causing VPMS rupture and responsive release of CAT. *In vitro* experiments revealed that M-CAT-NGs effectively inhibited the proliferation of NTHi, *Staphylococcus aureus* (*S. aureus*), and *Escherichia coli* (*E. coli*), while also demonstrating the capacity to modulate the inflammatory response induced by lipopolysaccharide (LPS) and hydrogen peroxide (H_2O_2) stimulation. *In vivo* experiments demonstrated that nebulized inhalation of M-CAT-NGs was effective in reducing airway hyperresponsiveness (AHR), alleviating inflammation, downregulating the expression level of ROS in the lung tissues, thus enabling the effective management of neutrophilic asthma. Thus, the development of M-CAT-NGs has shown strong potential for the clinical management of neutrophilic asthma by modulating the inflammatory response.

Keywords Antibacterial nanogels, Inflammatory modulation, MMP-9 responsive, Neutrophilic asthma

*Correspondence:
Caina Xu
xucaina@jlu.edu.cn
Chaoliang He
clhe@ciac.ac.cn
Fang Wang
wf@jlu.edu.cn

[1]College of Basic Medical Sciences, the Medical Basic Research Innovation Center of Airway Disease in North China, Key Laboratory of Pathobiology, Ministry of Education, Jilin University, Changchun 130021, China
[2]Key Laboratory of Polymer Ecomaterials, Changchun Institute of Applied Chemistry, Chinese Academy of Sciences, Changchun 130022, China
[3]Key Laboratory of Pathobiology, Ministry of Education, College of Basic Medical Sciences, Jilin University, Changchun 130021, China
[4]Cross-disciplinary Innovation Center, Jilin University, Changchun 130021, China

Introduction

Asthma is a chronic, heterogeneous disease marked by persistent airway inflammation triggered by environmental factors and allergens. The intricate interplay between genetic predisposition and environmental exposures has positioned asthma among the most challenging non-communicable diseases globally [1, 2]. Asthma is typically characterized by symptoms including coughing, wheezing, chest tightness, and breathlessness [3, 4]. Inhaled corticosteroids (ICS) and bronchodilators remain the current mainstay of clinical treatment of asthma and can alleviate symptoms in most patients, but even with high doses of ICS and/or long-term oral corticosteroids (OCS), approximately 5–10% of asthma patients still experience no improvement in symptoms [5–7]. Studies have shown that these patients typically exhibit a markedly elevated neutrophil percentage, demonstrate resistance to corticosteroid therapy, and suffer from a severe disease course associated with high hospitalization and mortality rates. This form of asthma, often triggered by infections, is referred to as neutrophilic asthma [8, 9]. Currently, there are no recognized therapeutic strategies for neutrophilic asthma. Therefore, it is crucial to foster the development of innovative therapeutics and strategies aimed at addressing neutrophilic asthma.

Neutrophilic asthma has been associated with a disruption in the balance of the pulmonary microbial ecosystem [10–13]. In particular, an elevated abundance of potentially pathogenic *Proteobacteria* (e.g., nontypeable *Haemophilus influenzae* (NTHi)) is closely linked to the manifestation of a severe neutrophilic asthma phenotype [14–16]. NTHi strains are infrequently associated with diseases beyond the respiratory tract and are regarded as primary pathogens of the respiratory mucosa. These bacteria can impair ciliary function and interact with mucus, facilitating their adhesion to the mucosal surfaces of the respiratory tract [17, 18]. NTHi has excellent ability to evade mucosal immunity and invasion, and can enter local respiratory tract tissues, survive within cells, and colonize within the respiratory tract [19]. Meanwhile, reactive oxygen species (ROS) are produced abundantly in neutrophils and macrophages and continue to be produced with NTHi infection [20]. High levels of ROS can further activate some inflammatory pathways, leading to the increase of inflammation levels in vivo [21]. Therefore, antibacterial therapy and modulation of the inflammatory response are very necessary for the management of neutrophilic asthma. In addition, researches have demonstrated that within the microenvironment of respiratory diseases, the concentration of matrix metalloproteinase-9 (MMP-9) mainly secreted by neutrophils and macrophages is higher than that in the normal environment [22]. MMP-9 can further lead to sustained neutrophil recruitment and exacerbate asthma symptoms by disrupting normal alveolar structure and promoting airway inflammation, mucus production and airway remodeling [23, 24]. Therefore, ROS and MMP-9 represent crucial therapeutic targets in the management of neutrophilic asthma, and nanomedicines can be reasonably designed based on ROS and MMP-9 to treat neutrophilic asthma.

Oxidative stress is intricately associated with the pathogenesis of asthma, playing a pivotal role in the development of airway hyperresponsiveness, airway remodeling, neutrophilic inflammation and the emergence of corticosteroid resistance [25]. Oxidative stress is commonly recognized as a signaling mechanism for many cellular processes, including proliferation, senescence, differentiation, signaling, transcription factor activation, and apoptosis [26]. As pro-oxidants, ROS contain hydroxyl radicals (·OH), superoxide anion ($\cdot O_2^-$), and hydrogen peroxide (H_2O_2), etc. $\cdot O_2^-$, one of the most common ROS, can be very rapidly converted to H_2O_2 and O_2 by a reaction catalyzed by superoxide dismutase (SOD) [27]. Under the catalysis of eosinophil and neutrophil peroxidases, H_2O_2 interacts with halides to form hypohalites, hypobromous acid (HOBr), and hypochlorous acid (HOCl), which then damage epithelial cells and promote the onset and development of asthma [28]. Therefore, scavenging H_2O_2 and thus reducing the accumulation of ROS in vivo is essential for the treatment of asthma. Catalase (CAT), the most abundant antioxidant enzyme in the body, is commonly found in the liver, alveolar epithelial cells, and erythrocytes, and serves as the most efficient catalyst for the decomposition of H_2O_2 [29]. However, native CAT is typically characterized by inherent instability and a remarkably brief half-life in vivo. Recently, scientists have increasingly turned to nanotechnology as a means to safeguard CAT, enabling its stable delivery to diseased tissues where it can exert its therapeutic effects [30].

It was reported that positively charged Chitosan (CS) not only exhibited antibacterial effects but also interacted with negatively charged mucoproteins in tracheal mucus, thereby prolonging the retention time of drugs on the mucosal surface [31]. The antibacterial activity could be further enhanced by modifying the side chains of CS with L-arginine (Arg). Arg could exert antibacterial activity by altering membrane permeability through proton motive force interference and inducing intracellular acidification [32]. In view of the pathophysiological mechanism of the increased expression of MMP-9 in the lung tissues of patients with neutrophil asthma, we selected MMP-9-sensitive peptide (Ac-GCRDVPMS↓MR GGDRCG (VPMS, Figure S1) as one of the components for the synthesis of nanogels. In addition, 3-maleimidopropionic acid N-hydroxysuccinimide ester (Mal) provided cross-linking sites between CS-Arg and VPMS, while sodium

citrate (SC) engaged in ionic interactions with CS-Arg, serving a physical cross-linking function. Besides, ε-PLL exerted its bactericidal effects through two primary mechanisms: (i) The cationic properties of ε-PLL enable electrostatic interaction with negatively charged bacterial membranes, compromising membrane integrity and inducing cytoplasmic leakage; (ii) It disrupts critical metabolic processes, ultimately inhibiting bacterial growth and proliferation [33]. Furthermore, CAT could exert its potent antioxidant effects through a highly efficient catalytic mechanism. The enzyme's heme prosthetic group (Fe^{3+}-protoporphyrin IX complex) directly decomposes cytotoxic H_2O_2 into water and molecular oxygen, making it one of nature's most efficient antioxidant systems [34]. Therefore, we built MMP-9-responsive, catalase-loaded nanogels (M-CAT-NGs) through ionic crosslinking and chemical conjugation (Scheme 1), which consisted of Arg and Mal grafted CS (CS-Arg-Mal), CAT, VPMS, SC and ε-PLL. The M-CAT-NGs were designed to possess the following advantages: (1) protecting CAT from degradation and improving bioavailability *in vivo*; (2) MMP-9 responsiveness, which could release CAT in response to the asthma environment, while reducing the content of MMP-9 and improving the treatment effect; (3) excellent antimicrobial properties and the ability to inhibit bacterial infections in asthma environments due to the presence of Arg and ε-PLL; (4) excellent ROS scavenging ability, which could regulate the inflammatory response and improve the inflammatory state. Nebulized inhalation of M-CAT-NGs could significantly reduce airway hyperresponsiveness, alleviate the inflammatory state and achieve a significant therapeutic effect on neutrophilic asthma mice. The adoption of this strategy has demonstrated promising potential in the management of neutrophilic asthma, paving the way for the clinical application of polymer-based nanomedicines in its management.

Materials and methods

Materials and agents

CS, Arg, 2-(N-morpholino)ethanesulfonic acid (MES) monohydrate, N-(3-(dimethylamino)propyl)-N′-ethylcarbodiimide hydrochloride (EDC·HCl), N-hydroxysuccinimide (NHS), Mal-NHS, ε-PLL, albumin from chicken egg white (OVA), amikacin disulfate and sodium citrate were provided by Aladdin Reagent. Aluminum hydroxide ($Al(OH)_3$), CAT and acetyl-β-methylcholine chloride were purchased from Sigma-Aldrich. VPMS and Ac-GCRDVpMSmRGGDRCG (p is D-Pro, m is D-Met, VpMS) were synthesized by ChinaPeptides Co., Ltd. MMP-9 protein and Cy5-NHS were provided by MedChemExpress. *Staphylococcus aureus* (*S. aureus*, ATCC 25923), *Escherichia coli* (*E. coli*, ATCC 25922) and Non-typeable *Haemophilus influenzae* (NTHi, ATCC 49247) were provided by Basic Medical Sciences College, Jilin University. The Cell Counting Kit-8 (CCK-8) was

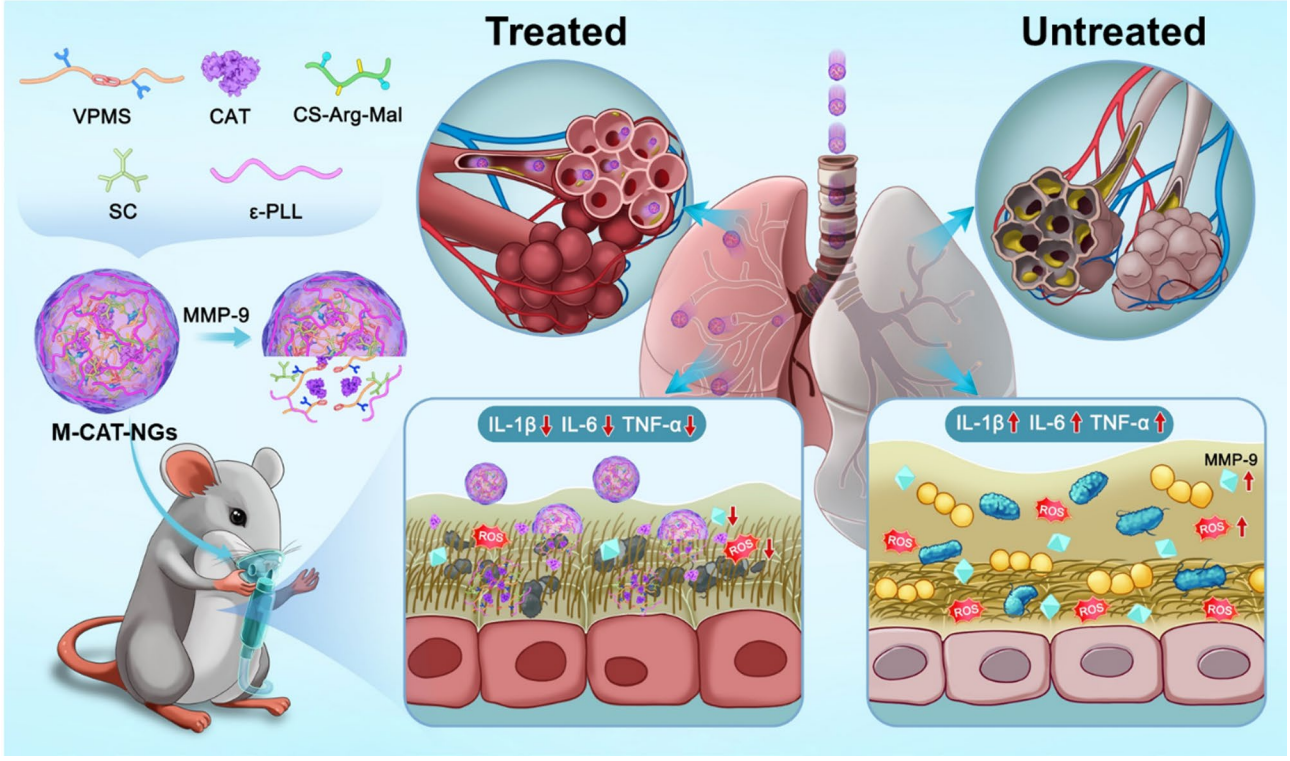

Scheme 1 Schematic illustration of MMP-9-responsive, catalase-loaded nanogels (M-CAT-NGs) for the management of neutrophilic asthma

obtained from Dojindo Laboratories, while ELISA kits for mouse IL-6, IL-1β, and TNF-α were obtained from Invitrogen. All antibodies used for flow cytometry were supplied by BD Biosciences.

Synthesis and characterization of CS-Arg-Mal

MES monohydrate was first dissolved in ultrapure water, followed by the addition of Arg into the MES solution. Then, EDC·HCl and NHS were added sequentially to the solution. The mixture was subjected to stirring for 2 h to facilitate the activation of Arg with NHS. Meanwhile, CS was introduced into the MES solution and stirred. After that HCl was gradually added until complete dissolution of CS was achieved. Following this, the activated Arg solution was gradually incorporated into the CS solution. The resulting mixture was then stirred continuously for 48 h. Then, the resulting solution was then dialyzed against deionized water for 72 h, followed by lyophilization to obtain the final product. The lyophilized product was taken and reconstituted with water to adjust the pH to acidic range. Mal-NHS was first dissolved in DMSO and subsequently introduced into the aqueous solution containing the lyophilized product from the preceding step. The reaction was then allowed to proceed for 36 h. Afterwards, the product was dialyzed in water and lyophilized to obtain CS-Arg-Mal.

CS, Arg, and CS-Arg-Mal were dissolved in D_2O, while Mal-NHS was solubilized in DMSO. The ^1H NMR spectra of CS, Arg, Mal-NHS, and CS-Arg-Mal were acquired at 500 MHz using a Bruker spectrometer. KBr was blended with CS, Arg, Mal-NHS, or CS-Arg-Mal and compacted into a disk for Fourier transform infrared spectroscopy analysis. This was conducted using a Bruker Vertex 70 spectrometer, providing further evidence of the successful synthesis of CS-Arg-Mal.

Synthesis and characterization of M-CAT-NGs

As an example, 2.16 mg of a MMP-9-sensitive peptide crosslinker, Ac-GCRDVPMS↓MRGGDRCG (VPMS) or a MMP-9 insensitive peptide control, Ac-GCRD-VpMSmRGGDRCG (VpMS, by converting the amino acids in the critical site to D-isoform (indicated by lowercase letters)), was dissolved in 2 mL of water as solution I [35]. 7.2 mg of CAT was dissolved in 2 mL of water as solution II. 7.2 mg of CS-Arg-Mal was dissolved in 4 mL of water to obtain solution III. 7.2 mg of SC was dissolved in 8 mL of water as solution IV. 7.2 mg of ε-PLL was dissolved in 16 mL of water as solution V. Solutions II to V were sequentially added to solution I. The mixed solution was allowed to stir thoroughly, and the pH was adjusted to 7 to obtain M-CAT-NGs (32 mL, the negative control was called CAT-NGs). The synthesis method of M-NGs was the same as that of M-CAT-NGs except that CAT was not added. The size distribution and zeta potential were assessed using dynamic light scattering (DLS). And the diameter and morphology were evaluated by TEM.

Enzymatic digestion of VPMS by MMP-9

MMP-9 was activated by APMA (4-aminophenylmercury acetate) in TCNB buffer. VPMS was dissolved in TCNB solution (20 μM, 200 μL) and then added to 200 μL of TCNB buffer containing active MMP-9 (0.4 mM). The VPMS fragments after enzymatic digestion were determined by HPLC-MS.

In vitro release assay of M-CAT-NGs

To investigate the stimuli-responsive drug release behavior of the nanogels, the *in vitro* release profile of CAT from M-CAT-NGs was assessed using a dialysis method in the presence or absence of MMP-9. Briefly, 1 mL of M-CAT-NGs mixed with MMP-9 was loaded into a dialysis bag (MWCO: 500 kDa) and immersed in 100 mL of PBS (pH 7.4) under gentle agitation using a magnetic stirrer. At predetermined time intervals (1, 2, 3, 4, 5, 6, 7, 8, 12, 24, and 48 h), 1 mL of the release medium was collected and replaced with an equal volume of fresh PBS. A control group without MMP-9 was established to investigate the basal release profile of M-CAT-NGs under non-stimulated conditions. Additionally, a group containing only MMP-9 group was included to account for potential interference from the enzyme. Under the conditions of containing MMP-9 and without MMP-9, the CAT released by M-CAT-NGs was quantitatively determined by the BCA method. Furthermore, a group containing only MMP-9 was added to eliminate the potential interference of this enzyme. The BCA method was used to quantify the CAT released by M-CAT-NG in the presence and absence of MMP-9.

Stability and enzyme activity test

To explore the stability of the nanogels over time, the particle size changes of M-CAT-NGs and M-NGs were tested, respectively. The enzyme activities of the samples were evaluated by using the rate of H_2O_2 decomposition after incubation with different samples. Briefly, 1.5 mL of PBS, 0.1 mL of the sample, 1.2 mL of water, 0.2 mL of H_2O_2 were added to the centrifuge tube sequentially, and 1 mL of 0.5 M H_2SO_4 was added after 4 min as the experimental group. For the control group, 1.5 mL of PBS, 0.1 mL of the sample, 1.2 mL of water, 1 mL of 0.5 M H_2SO_4, 0.2 mL of H_2O_2 were added to the centrifuge tube sequentially. The absorbance of the solution was subsequently assessed at 240 nm, with the difference reflecting the decomposition of H_2O_2.

Fluorescent measurement of intracellular ROS

RAW264.7 cells were subsequently loaded with 5 μM of 2,7-dichlorodihydrofluorescein diacetate (DCFH-DA) in

phosphate-buffered saline (PBS) and incubated at 37 °C for 25 min. Fluorescence was then assessed at excitation and emission wavelengths of 485 nm and 530 nm, respectively.

In vitro cytotoxicity test

L929, RAW264.7, and Beas-2b cells were individually cultured in DMEM medium. Cells in the logarithmic phase were harvested and seeded into 96-well plates. Following this incubation period, the medium was removed, and various solutions were added to the wells for co-incubation with the cells. Cell viability was assessed after 24–48 h using the CCK-8 reagent, following the manufacturer's instructions.

In vitro ROS test

Cell viability was assayed by CCK-8 to select an appropriate H_2O_2 concentration to stimulate Beas-2b and RAW264.7 cells to produce ROS. The cells were then co-incubated with 0.96 mg/mL of M-NGs or CAT or CAT-NGs or M-CAT-NGs, respectively. Ultimately, the cells were incubated with 5 μM of DCFH-DA in PBS. Microplate reader and fluorescence microscopy were used to observe the remaining intracellular ROS.

Cellular uptake test

M-CAT-FITC-NGs were synthesized to explore cellular uptake of nanogels. The specific methods were as follows: 20 mg of CAT and 3 mg of FITC were dissolved in 5.6 mL of alkaline buffer and 1.5 mL of DMSO, respectively. Subsequently, the FITC solution was added to the CAT solution. The resulting solution was dialyzed in PBS for three days, followed by freeze-drying to get CAT-FITC. The preparation method for M-CAT-FITC-NGs was the same as the method described above for CAT-FITC. RAW264.7 cells were incubated with CAT-FITC and M-CAT-FITC-NGs for 12 h, and after treating the cells with Hoechst 33,342 as a nuclear dye, observed under a confocal laser scanning microscope (CLSM).

In vitro anti-inflammatory test

RAW264.7 cells were stimulated using 1 μg/mL LPS and then the supernatant was removed. 0.36 mg/mL of M-NGs or CAT or M-CAT-NGs was added to the cell culture flasks for 24 h and then the cell supernatants were harvested for ELISA analysis.

Antibacterial test

In this study, the antimicrobial effect of the M-CAT-NGs was verified using NTHi, *E. coli*, and *S. aureus*. The antibacterial efficacy of CS-Arg-Mal, CAT, ε-PLL, M-NGs, and M-CAT-NGs was evaluated through the minimum inhibitory concentration (MIC) test and bacterial live-dead staining, among other methods. In the MIC assay, 1×10^6 CFU/mL of NTHi, *E. coli*, or *S. aureus* was co-incubated with varying concentrations of the samples using a two-fold dilution technique. After a designated incubation period, the absorbance at 600 nm was measured to ascertain the MIC. The antibacterial activity against the above three bacteria was investigated in a coated plate counting assay using 0.48 mg/mL of the samples. Bacteria were co-cultured with a mixture of PBS or M-CAT-NGs for 24 h and subsequently subjected to serial dilutions using a ten-fold gradient. A volume of 20 μL from each diluted solution was evenly spread on agar plates and incubated for a specified duration. The colonies that formed were counted to assess the bacterial inhibitory efficacy of M-CAT-NGs.

To obtain scanning electron microscope (SEM) images, bacterial solutions co-incubated with PBS or nanogels were subjected to dehydration using a gradient of ethanol (25%, 50%, and 75%). The bacteria were then resuspended in anhydrous ethanol, and the resulting suspension was deposited onto a silicon wafer to dry before imaging. Furthermore, the co-incubation culture mixtures were resuspended in PBS, and washed three times. Subsequently, staining was performed using a bacterial live-dead staining kit for 30 min, followed by imaging with a fluorescence microscope.

Establishment of murine model

All animal experiments were conducted in accordance with the guidelines sanctioned by the Animal Care and Use Review Committee of Jilin University and received approval from the Animal Ethics Committee of the College of Basic Medical Sciences at Jilin University (No. 2023 – 444). Female BALB/c mice (6–8 w) were divided into 6 groups ($n = 6$), including NC (normal control group), OVA&NTHi (OVA, NHTi, and PBS treatment group), M-NGs (OVA, NHTi, and empty material group without encapsulated catalase treatment group), CAT (OVA, NHTi, and native catalase treatment group), M-CAT-NGs (OVA, NHTi, and M-CAT-NGs treatment group), and AM (OVA, NHTi, and amikacin treatment group). On days 0, 7, and 14, mice in the OVA&NTHi, M-NGs, CAT, M-CAT-NGs, and AM groups were sensitized with $Al(OH)_3$ and OVA. In parallel, the NC group received an equivalent volume of sterile saline. Between days 21 and 23, mice in the OVA&NTHi, M-NGs, CAT, M-CAT-NGs, and AM groups were subjected to daily challenges with OVA solution. Mice in the NC group underwent sham sensitization and were similarly challenged with equal volumes of saline. On day 24, all mice were anesthetized with pentobarbital; those in the OVA&NTHi, M-NGs, CAT, M-CAT-NGs, and AM groups were inoculated intratracheally with NTHi (10^6 CFU/mL, 30 μL saline), while the NC group received the same volume of sterile saline. From days 25 to 27, the

NC and OVA&NTHi groups were nebulized with sterile saline for 30 min daily; mice in the M-NGs group were nebulized with 0.96 mg/mL of M-NGs for 30 min daily; those in the CAT group received 0.96 mg/mL of catalase under the same conditions for 30 min daily, mice in the M-CAT-NGs group were nebulized with 0.96 mg/mL of M-CAT-NGs for 30 min daily, and mice in the AM group were nebulized with 0.2 mg/mL of amikacin for 30 min daily. On day 28, all mice were anesthetized and euthanized in preparation for subsequent experiments.

Biodistribution of free CAT and M-CAT-NGs in mice

BALB/c mice (6–8 w, $n = 6$) were nebulized with CAT-FITC and M-CAT-FITC-NGs (synthesized in the same way as the Cellular Uptake Test section) for 30 min, and were euthanized 1 h, 12 h and 24 h post-nebulization. The organs of the mice were harvested and subsequently imaged using an *in vivo* imaging system (IVIS Spectrum, Perkin Elmer).

Collection of BALF

The mouse trachea was meticulously dissected and connected to a syringe containing sterile PBS, allowing the lung lumen to be thoroughly flushed with PBS three consecutive times. The recovered fluid was centrifuged and the precipitated cells were taken for flow cytometry.

Flow cytometry

Cells isolated from the BALF were labeled with antibodies. The mixture was agitated three times at 10 min intervals, after which the labeling process was halted with PBS. The labeled cells were subsequently analyzed using flow cytometry.

ELISAs test

The levels of IL-6, IL-1β, and TNF-α in both cell culture supernatants and lung tissues were quantified using ELISA kits. All procedures were performed following the guidelines provided by the manufacturer and repeated three times.

Lung function measurement

Lung function test was conducted using the Buxco pulmonary function testing system [36, 37]. Briefly, the mice were anesthetized and tracheally intubated, with their tracheas connected to the machine's spirometer, barometric pressure sensor, and pressure sensor. Subsequently, the mice were exposed to varying concentrations of acetylcholine, while lung function parameters were automatically assessed by the spirometer.

In vivo ROS test

Mouse lungs were collected, frozen and sectioned, and after quenching tissue autofluorescence, the tissues were incubated with ROS staining solution (37 °C, 30 min) and DAPI staining solution (37 °C, 5 min) in a light-proof incubator. Then the tissues were blocked and photographed.

In vivo safety evaluation

Female BALB/c mice were randomized into 4 groups ($n = 6$) to assess the *in vivo* safety of M-CAT-NGs. NC mice were nebulized with saline. Simultaneously, the other three groups of mice were subjected to daily nebulization with 0.96 mg/mL of M-NGs, CAT, and M-CAT-NGs, respectively. On day 3, all mice were euthanized, and the blood were collected to assess liver and kidney functions. Major organs were harvested for Hematoxylin-Eosin (H&E) staining.

H&E staining

The lungs of the mice were harvested. Then, the lungs were fixed with paraformaldehyde, embedded in paraffin, and subsequently sectioned. The paraffin sections were then stained with hematoxylin and eosin to evaluate the histopathological features.

Alcian blue periodic acid schiff (AB-PAS) staining

Similar to H&E Staining, the lungs of the mice were collected and fixed with paraformaldehyde. The fixed tissues were embedded in paraffin, sectioned, and subsequently stained with AB-PAS to evaluate mucus secretion in the lungs.

Statistical analysis

The results are presented as the mean ± standard error of the mean (s.e.m.), as specified. The dataset was processed, and graphics were generated using Prism 9.0 and OriginPro 8.1. Paired t-tests and one-way analysis of variance (ANOVA) were employed for multiple comparisons when more than two groups were analyzed. A p-value of less than 0.05 was considered statistically significant.

Result and discussion

Synthesize and characterization of M-CAT-NGs

The M-CAT-NGs synthesis route was shown in Fig. 1a. The synthetic route of CS-Arg-Mal was shown in Fig. S2. ^{1}H NMR spectra (Fig. S3) demonstrated that Arg and Mal could be successfully conjugated with CS backbone by EDC/NHS coupling chemistry. The signal peaks at 3.25–3.48 ppm (e'), 1.43–1.85 ppm (d'), and 2.28–2.51 ppm (c') represented the three methylene groups in Arg, and the signal peak at 6.74–6.87 pm (i') represented the carbon-carbon double bond of Mal. The FTIR spectra of CS, Arg, Mal and CS-Arg-Mal were shown in Fig. 1b. In the spectra of CS-Arg-Mal, a characteristic peak at 1701 cm^{-1} indicating the carbon-oxygen double bond in Mal, an absorption peak at 1630 cm^{-1} indicating the

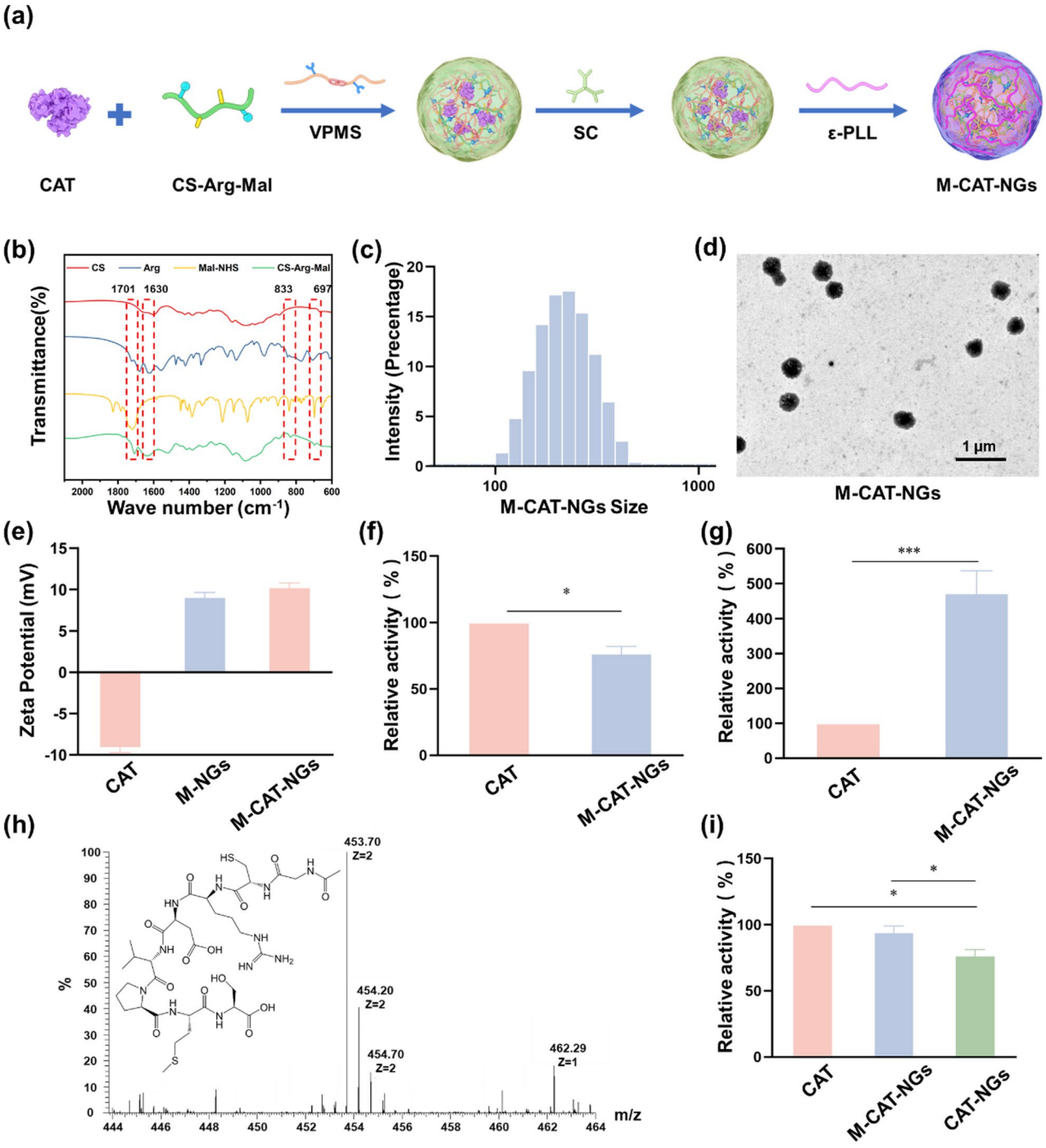

Fig. 1 (**a**) Synthesis route of M-CAT-NGs. (**b**) FTIR spectra of CS, Arg, Mal-NHS and CS-Arg-Mal. (**c**) Size distribution analysis of M-CAT-NGs suspended in PBS, as determined using a Malvern Nano-ZS90 ($n=3$). (**d**) TEM image of M-CAT-NGs. (**e**) Zeta potentials of CAT, M-NGs and M-CAT-NGs ($n=3$). (**f**) Relative enzyme activities of M-CAT-NGs and CAT ($n=3$). (**g**) Relative enzyme activities of CAT and M-CAT-NGs after 4 h of trypsin incubation. (**h**) The VPMS fragment cleaved by MMP-9, determined by UPLC-MS. (**i**) Relative enzyme activities of M-CAT-NGs and CAT-NGs relative to CAT in the presence of MMP-9 ($n=3$), $^{*}p<0.05$, $^{***}p<0.001$

presence of guanidinium group, and characteristic peaks at 833 cm^{-1} and 697 cm^{-1} representing the carbon-carbon double bond in Mal were observed.

The size distribution of CAT was centered at 639.3 ± 9.7 nm, M-NGs was centered at 164.1 nm and that of M-CAT-NGs was centered at 199.3 nm (Fig. S4-5, Fig. 1c). The TEM results showed that the size of M-CAT-NGs was approximately 129.8 nm (Fig. 1d), which was marginally smaller than the values obtained through DLS analysis (Table S1). This discrepancy could be due to the

swelling of M-CAT-NGs in solution. The zeta potentials of CAT, M-NGs and M-CAT-NGs were − 9.17 mV, 9.1 mV and 10.3 mV (as shown in Fig. 1e, Table S1). This was a reassuring result, as it has been shown that positively charged nanoparticles typically achieve superior internalization and enhanced cellular uptake efficiency compared to their negatively charged nanoparticles [38]. These results demonstrated that nanoencapsulation of CAT yields uniformly sized particles with reversed surface charge (from negative to positive), both of which were advantageous for subsequent *in vivo* experiment.

To investigate the stimuli-responsive drug release behavior of the nanogels, the *in vitro* release profile of CAT from M-CAT-NGs was assessed using a dialysis method in the presence or absence of MMP-9. As demonstrated in Fig. S6, M-CAT-NGs exhibited MMP-9-dependent release kinetics, with approximately 80% of CAT released within 10 h under MMP-9-present conditions. In contrast, the release was significantly slower in the absence of MMP-9, with minimal detectable release during the initial 3 h and only ~ 25% cumulative release by 48 h. The size distribution of the M-CAT-NGs was determined in PBS to evaluate their stability. DLS characterization demonstrated that after 7 days of incubation, there was no significant variation in the particle size of the M-CAT-NGs, indicating that the M-CAT-NGs had good physiological stability in PBS (Fig. S7). The relative enzyme activities of M-CAT-NGs and CAT were shown in Fig. 1f. The results revealed that the enzyme activity of M-CAT-NGs could reach about 80%, which might be caused by the incomplete release of CAT within the nanogels within a brief time frame. In addition, to assess the protective efficacy of the nanogel on catalase activity, CAT and M-CAT-NGs were incubated with trypsin for 4 h, after which their relative enzymatic activities were assessed. As shown in Fig. 1g, after 4 h of trypsin incubation, the enzymatic activity in the M-CAT-NGs group surpassed that of the native CAT group by over 400-fold. The results indicated that the outer layer of nanogels could well protect the enzymatic activity of CAT, which was essential to protect the activity of catalase from the complex environment *in vivo*.

To evaluate the sensitivity of VPMS to MMP-9 [31], the enzymatic cleavage of VPMS was investigated. As shown in Fig. 1h, the main fragment (Ac-GCRD-VPMS = 453.70, Z = 2) cleaved by MMP-9 was identified by ultra-performance liquid chromatography-mass spectrometry (UPLC-MS). Moreover, MMP-9-insensitive peptide (VpMS) was used to replace VPMS to prepare MMP-9-insensitive nanogels (CAT-NGs), and detect the effect of MMP-9 on enzyme activity in MMP-9-sensitive nanogels (M-CAT-NGs) and MMP-9-insensitive nanogels (CAT-NGs). When MMP-9 was added, the enzyme activity of M-CAT-NGs was not significantly different from that of native CAT, whereas the enzyme activity of CAT-NGs was significantly decreased compared to that of native CAT (Fig. 1i). The above results reconfirmed that VPMS could be cleaved by MMP-9, thus enabling M-CAT-NGs to sensitively release CAT.

In vitro anti-inflammatory test

Since the potential toxicity of nanomedicines is a point of contention for their biomedical applications [39], multiple cell lines were utilized to evaluate their *in vitro* biocompatibility. The survival of L929, RAW264.7 and Beas-2b cells was evaluated by CCK-8 assay after treatment with different samples. As shown in Fig. S8, the evaluation of cell viability following 24 h of co-culture revealed that all material concentrations below 480 μg/mL exerted no significant effect on the viability of any of the three cell lines. When the time was extended to 48 h, some of the samples at the concentration of 420 μg /mL and over exhibited reduction in cell viability, probably due to the toxic effects caused by the accumulation of nanogels ingested into the cells with increasing time. Therefore, to ensure the safety of the nanogels, the concentration of 360 μg/mL was used for the following i*n vitro* experiments.

Additionally, CLSM was utilized to observe the uptake of CAT-FITC and M-CAT-FITC-NGs by Beas-2b and RAW264.7 cells. The fluorescence images in Fig. 2a demonstrated that M-CAT-FITC-NGs were more readily taken up by Beas-2b cells compared to CAT-FITC, which could be attributed to the nanogel shell providing favorable solubility and positively-charged surface for endocytosis [40]. A similar trend was observed in RAW264.7 cells, where M-CAT-FITC-NGs exhibited easier uptake by cells than CAT-FITC, further supporting the role of the nanogels formulation in improving drug delivery efficiency (Fig. S9).

ROS are exacerbated during severe asthma and acute exacerbations, which may lead to oxidative damage to tissues, promoting airway inflammation and hyperresponsiveness [28]. H_2O_2 is a key metabolite of oxidative stress, and high concentrations of H_2O_2 can induce inflammatory responses that lead to growth arrest and death of cells [41]. Therefore, to preliminarily investigate the anti-inflammatory effect of nanogels, H_2O_2-stimulated Beas-2b and RAW264.7 cells were used. Based on CCK-8 results, 1 mmol/L H_2O_2 was used to stimulate both Beas-2b and RAW264.7 cells (Fig. S10-11). The level of intracellular ROS was significantly decreased in the Beas-2b cells of the M-CAT-NGs group and CAT group compared to the H_2O_2 stimulation alone group (Fig. 2b, Fig. S12). There were higher intracellular ROS levels in the CAT-NGs group compared to the M-CAT-NGs group. This might be due to the lack of the ability of reactive release in CAT-NGs, which resulted in slower kinetics

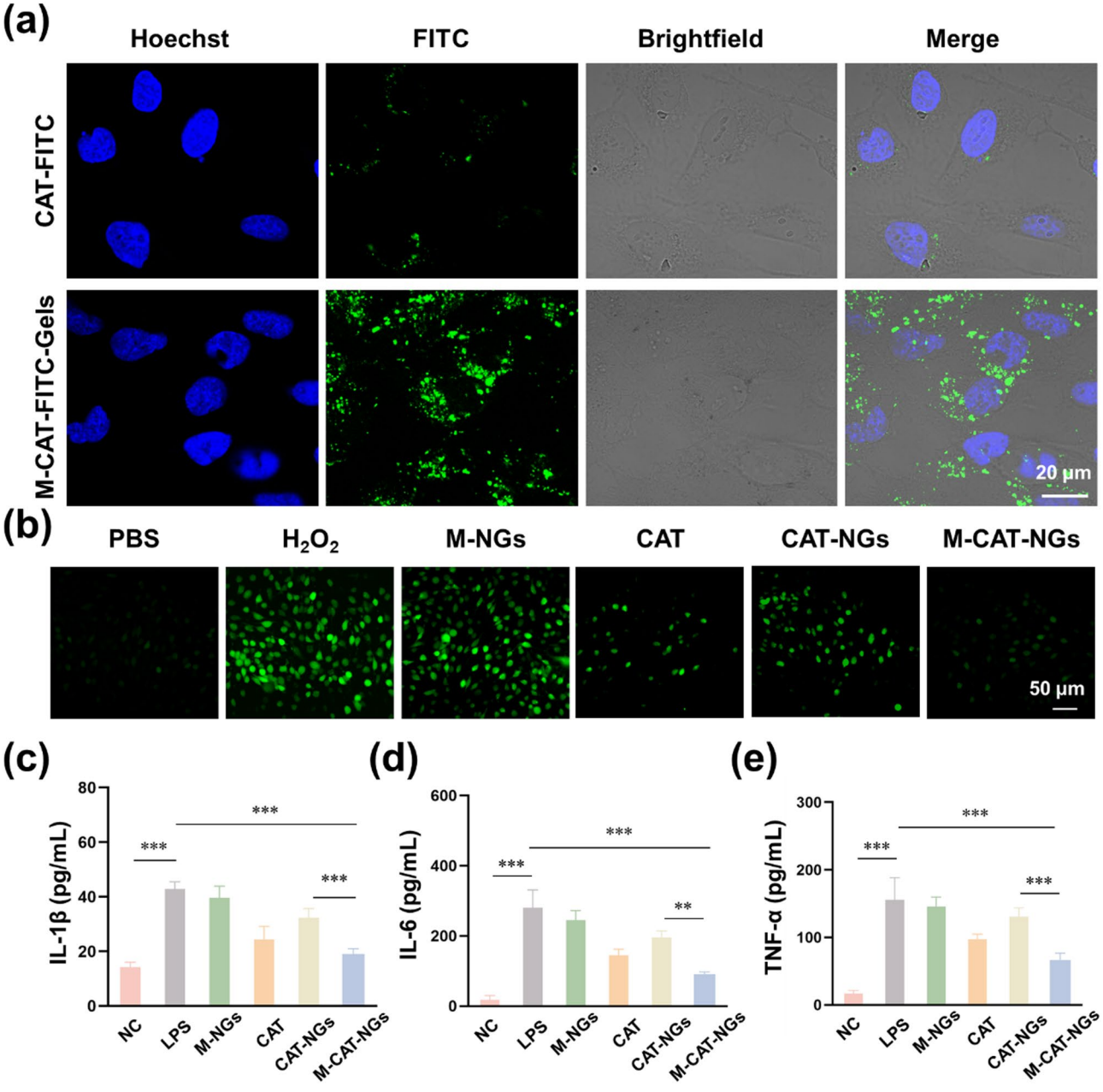

Fig. 2 (**a**) Cellular uptake of CAT-FITC and M-CAT-FITC-NGs on Beas-2b cells for 12 h, measured by CLSM. The scale bar in the image corresponding to each sample indicate a length of 20 μm. (**b**) Representative images of intracellular ROS in Beas-2b cells detected by the peroxide-sensitive probe DCFH-DA. The scale bar in the image corresponding to each sample indicate a length of 50 μm. (**c**-**e**) Expression levels of IL-1β, IL-6, and TNF-α in Beas-2b cells after different sample treatments ($n = 3$), $^{**}p < 0.01$, $^{***}p < 0.001$

of CAT release from the nanogels, leading to a less efficient ROS scavenging than that of M-CAT-NGs. However, there was no significant change in the M-NGs group compared to the H_2O_2 group. The result might be due to the fact that CAT was the main component to decompose H_2O_2. Since CAT was not contained in M-NGs, the ROS level of M-NGs treated cells remained comparable to that of the H_2O_2 group. Similar results were obtained using microplate reader to measure the relative expression of ROS in the above cells (Fig. S13). Notably, we observed similar trends in RAW264.7 cells (Fig. S14-S15).

Neutrophilic asthma is usually accompanied with bronchial inflammation. Toll like receptors (TLRs) are over-activated, leading to the release of large amounts of pro-inflammatory factors such as IL-6 and IL-1β, and aggravating the level of airway inflammation [42]. Meanwhile, activated neutrophils also secrete inflammatory factors such as TNF-α, further exacerbating airway

inflammation and promoting airway remodeling, leading to asthma exacerbation [43, 44]. Thus, regulating inflammation is crucial for the effective management of asthma [45]. To explore the anti-inflammatory effects of M-CAT-NGs, 1 μg/mL LPS was used to pre-stimulate Beas-2b and RAW264.7 cells for 12 h, followed by co-incubation of cells with different samples for 24 h. As shown in Fig. 2c-e, LPS stimulation of cells resulted in the production of high levels of IL-1β, IL-6, and TNF-α. The three inflammatory factors showed similar trends after treatment with different samples. Compared with the LPS group, there was no significant change in the inflammatory factors in the M-NGs and CAT-NGs groups, and the inflammatory factors in the CAT and M-CAT-NGs groups were reduced. Similar to what we observed in the ROS scavenging experiments, the anti-inflammatory capacity of the M-CAT-NGs group was better than that of the CAT-NGs group, which further confirmed the role of MMP-9 responsive release. Similar trends were observed in RAW264.7 cells (Fig. S16). The above results suggested that the M-CAT-NGs might have the ability to modulate inflammation, and therefore have a therapeutic potential for neutrophilic asthma.

Antibacterial test

Microbial infections have been implicated as significant contributors to the onset of neutropenic asthma, and in addition to viral infections, respiratory colonization by NTHi, *Staphylococcus aureus*, *Pseudomonas aeruginosa*, and *Catamorax* can exacerbate symptoms in patients with neutrophilic asthma [46–49]. Therefore, antimicrobial therapy is also essential in the management of neutrophilic asthma. The results of bacterial live-dead staining experiments showed that the vast majority of NTHi were killed after 24 h of co-incubation with M-CAT-NGs compared to the PBS control (Fig. 3a). The morphology of the bacteria in the different groups was further observed, most of the bacteria in the M-CAT-NGs-treated group lost their original morphology and showed crumpled and fragmented structures, indicating

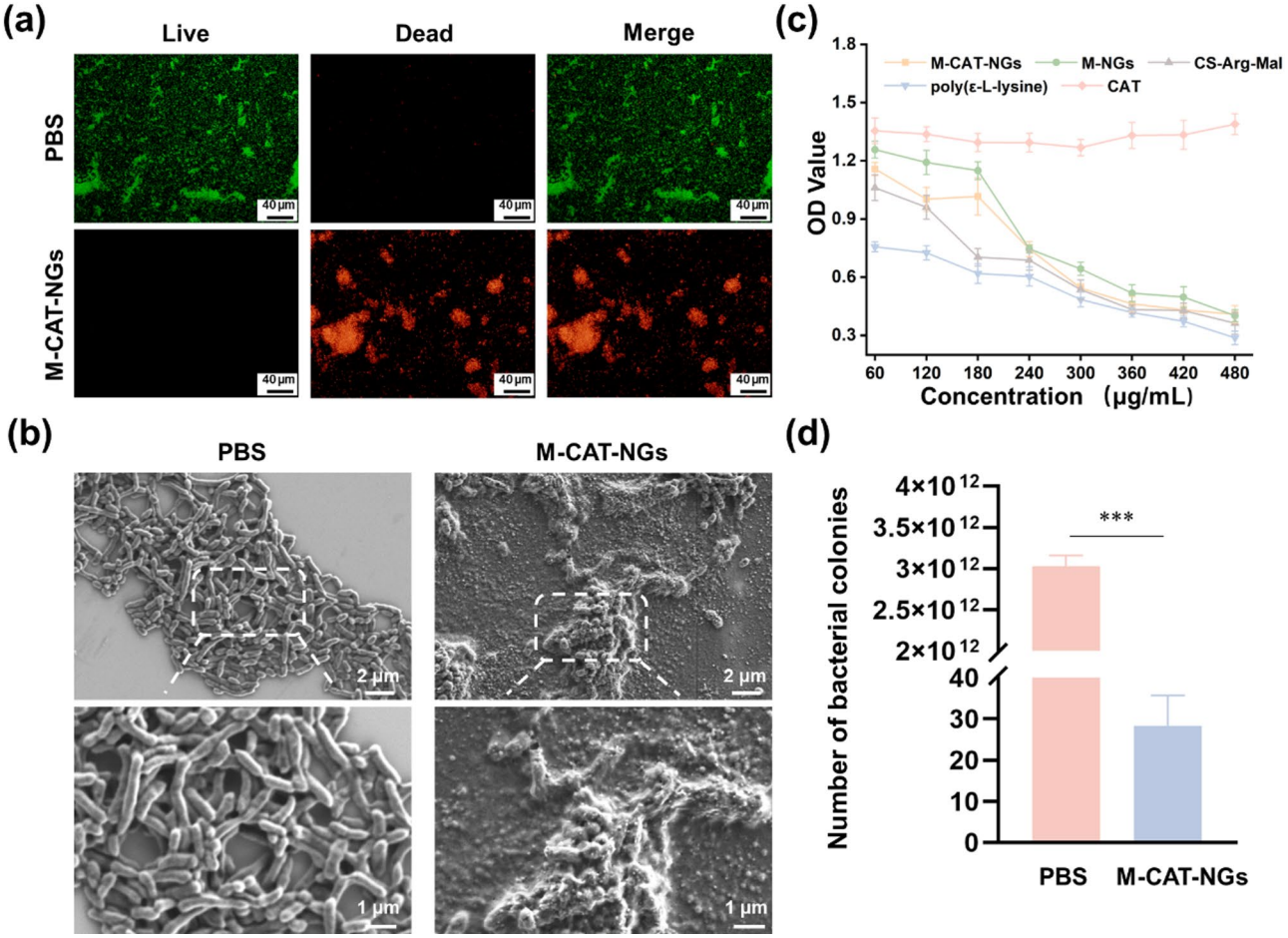

Fig. 3 (**a**) Live-Dead staining images of NTHi following incubation with either PBS or a 0.36 mg/mL M-CAT-NGs solution. The scale bars indicated a length of 40 μm. (**b**) SEM images of NTHi following a 24 h incubation with either PBS or a 0.36 mg/mL M-CAT-NGs solution were presented. The scale bars represented 2 μm and 1 μm, respectively. (**c**) Growth curves of NTHi incubated with different samples ($n = 3$). (**d**) Counts of colonies on agar plates coated with NTHi solution with different samples ($n = 3$), $^{***}p < 0.001$

that the nanogels might have exerted their antimicrobial effect by disrupting the bacterial structure (Fig. 3b). In addition, the growth of NTHi at different time points after co-culture of M-CAT-NGs or its different components with NTHi was measured using a microplate reader. As shown in Fig. 3c, except for the CAT group where the optical density (OD) value did not change much, the OD values of all groups decreased with the increase of sample concentration. The excellent bactericidal ability of M-CAT-NGs was further confirmed by the smear plate counting method, in which the bacterial solutions were taken out after co-incubation with PBS or M-CAT-NGs for 24 h and diluted separately (10^{14}-fold dilution for PBS group). The large number of bacteria killed in the M-CAT-NGs group could be confirmed by the counting results in Fig. 3d. In addition, similar results were obtained after incubation of M-CAT-NGs with *S. aureus* and *E. coli* (Fig. S17-18). The above results demonstrated that M-CAT-NGs had good antimicrobial capacity by destroying the bacterial structure, which might be attributed to its components with antimicrobial capacity, such as CS-Arg-Mal and ε-PLL. In fact, CS, Arg and ε-PLL have been reported to have good antimicrobial properties due to their positively charged moieties capable of binding to negatively charged compounds on the bacterial surface and disrupting the bacterial morphology [50–52]. Based on the experimental results above, it could be concluded that M-CAT-NGs possessed a strong inhibitory effect on different types of bacteria, indicating that M-CAT-NGs was expected to alleviate disease progression of patients with neutrophilic asthma by inhibiting bacterial growth.

Construction of *in vivo* model and therapeutic effects of M-CAT-NGs in mice

Studies have shown that NTHi was a dominant bacterium in the airway of severe asthma patients and that NTHi colonization in the airway was strongly correlated with the severity of asthma [53]. Therefore, to investigate whether M-CAT-NGs could alleviate the symptoms of neutrophilic asthma in mice, we established an animal model of neutrophilic asthma in mice sensitized by intraperitoneal injection of OVA and infected with NTHi. The method of constructing the animal model was referred to previous studies by our team, as shown in Fig. 4a [44]. Briefly, mice were sensitized by intraperitoneal injection of 50 μg OVA and 25 μL $Al(OH)_3$ per mouse on days 0, 7, and 14. From days 21 to 23, the mice were subjected to daily challenges with a 5% OVA solution for a duration of 45 min. In contrast, mice in the NC group were sham-sensitized with saline and subsequently challenged with an equivalent volume of saline. On day 24, NTHi (10^6 CFU, 20 μL) was inoculated into the trachea of anesthetized mice and an equal amount of saline was injected into the trachea of mice in the NC group. The mice were then treated with nebulized drug administration with PBS, M-NGs, CAT and M-CAT-NGs on days 25–27. Physiological indices were measured and samples were taken from the mice on day 28. As anticipated, the protein expression level of MMP-9 in lung tissues of the OVA&NTHi group was significantly elevated compared to the NC group (Fig. S19), further validating our material design strategy.

In vivo biodistribution and toxicity test

To explore the ability of M-CAT-NGs to accumulate in the lungs, the distribution and accumulation of CAT and M-CAT-NGs *in vivo* were evaluated in the neutrophilic asthma mice after nebulized inhalation. As shown in Fig. 4b-c, the M-CAT-FITC-NGs predominantly accumulated in lung and maintained strong fluorescence signals even 24 h after inhalation via nebulization. In contrast, 1 h after nebulization of CAT-FITC, relatively high accumulation of CAT-FITC was observed in the lung, liver, and kidney. By 24 h, the fluorescence signal of CAT-FITC in lung had significantly decreased (Fig. S20). These findings suggested that the nanogel shell substantially enhanced the lung retention of CAT, thereby reducing its distribution to other organs and lowering the risk of systemic side effects.

Airway hyperresponsiveness (AHR) test

AHR is considered a characteristic feature of asthma and the most widely used method to assess AHR is the methacholine inhalation provocation test [54]. Airway resistance (RI) and dynamic compliance (Cdyn) are important indices to assess AHR. Consequently, changes in RI and Cdyn with increasing doses of methacholine were investigated. As shown in Fig. 4d-e, RI in OVA&NTHi group was increased significantly compared to NC group, with the dose of methacholine rising. At a methacholine concentration up to 25 mg/mL, RI reached a maximum, implying that neutrophilic asthma mice showed respiratory distress. The elevated trend of RI was alleviated after M-NGs, M-CAT-NGs, and AM treatments. In addition, compared with mice in NC group, mice in OVA&NTHi group showed a significant decrease in Cdyn under treatments with different concentrations of methacholine, whereas Cdyn was significantly increased in both groups after M-NGs, M-CAT-NGs, and AM treatments (Fig. 4f-g). This indicated that M-NGs, M-CAT-NGs, and AM treatments alleviated dyspnea, enhanced respiratory depth and more effectively increased in expiratory volume in OVA&NTHi-treated mice [55]. The improvement effect of M-CAT-NGs on Cdyn appeared to be superior to that of AM, possibly due to the dual functions of M-CAT-NGs in antibacterial activity and ROS clearance, which contributed to enhanced lung function. Compared

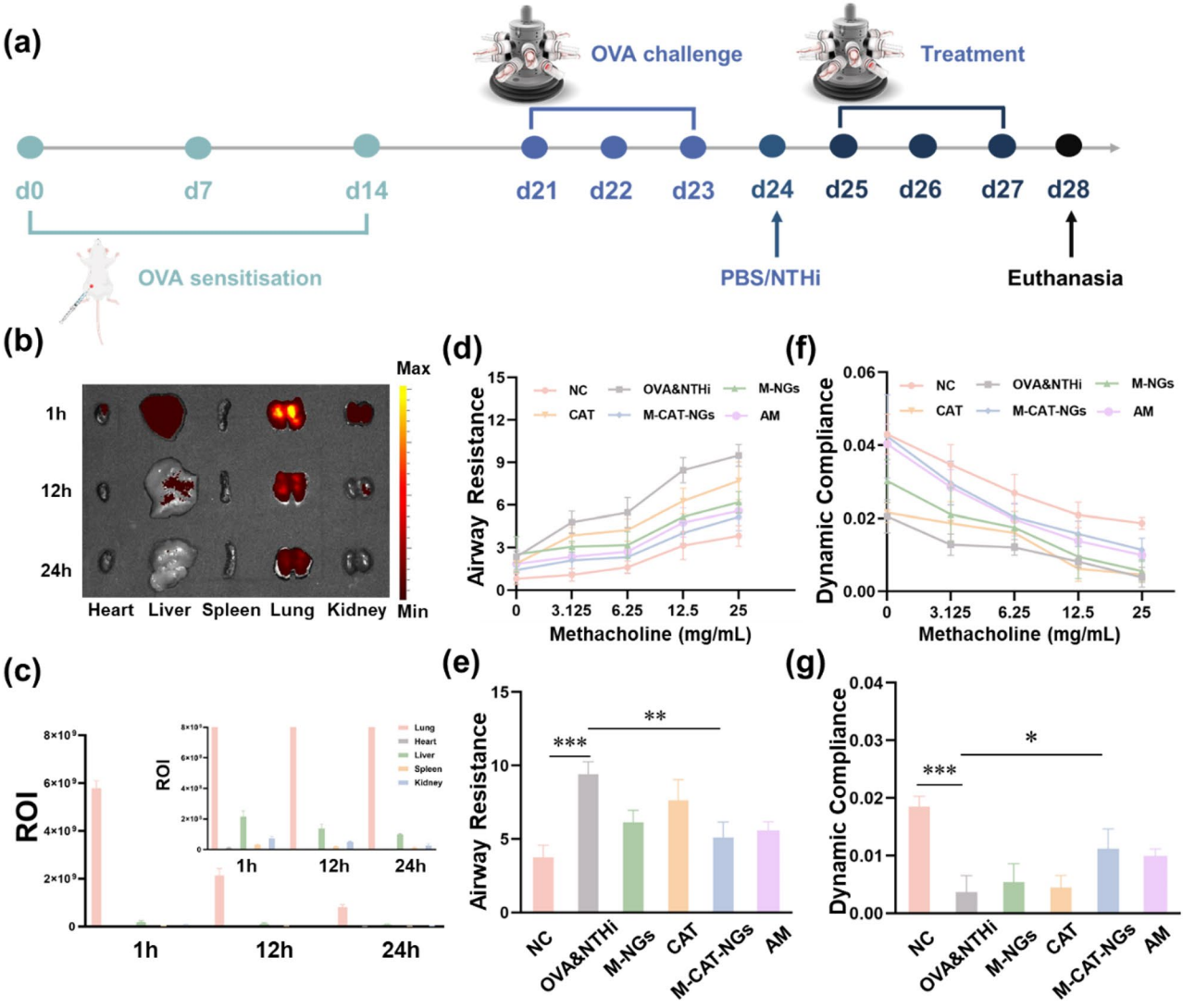

Fig. 4 (**a**) Schematic diagram of the establishment of the *in vivo* model along with the corresponding treatment protocol. (**b**) Fluorescence image of major tissues at 1, 12, and 24 h after nebulized M-CAT-FITC-NGs. (**c**) The statistics of (**b**). The insets of (**c**) represented local magnification. ROI: region of interest. (**d**) The variations in respiratory system resistance in response to various treatments. (**e**) The alterations in respiratory system resistance following treatment with 25 mg/mL methacholine ($n = 6$). (**f**) The modifications in lung dynamic compliance in response to various treatments. (**g**) The variations in lung dynamic compliance following administration of 25 mg/mL methacholine ($n = 6$), $^{*}p < 0.05$; $^{**}p < 0.01$; $^{***}p < 0.001$

with OVA&NTHi group, neither RI nor Cdyn changed significantly in CAT group, probably due to native CAT was unstable and susceptible to decomposition *in vivo*, while nanogels provided a protective effect to prevent CAT from losing its activity, and improved its solubility so that it could be more easily and efficiently nebulized for inhalation. These results suggested that neutrophilic asthma mice had a severe lung function deficit, as evidenced by high airway resistance and low dynamic lung compliance, which could be alleviated to some extent by M-CAT-NGs.

Modulation of the inflammatory response *in vivo* assay

To investigate whether M-CAT-NGs could exert a mitigating effect on airway inflammation in neutrophilic asthma mice, the proportion of neutrophils ($Ly6G^{+}$, $CD11b^{+}$) in BALF and inflammatory factors in lung tissue were examined. As shown in Fig. 5a-b, the proportion of neutrophils was significantly increased in the OVA&NHTi group compared with the NC group, whereas the proportion of neutrophils was significantly decreased in the M-NGs and M-CAT-NGs groups compared with the OVA&NHTi group, and there was no significant change in the proportion of neutrophils in the CAT group compared with the OVA&NHTi group. M-NGs and M-CAT-NGs could significantly reduce

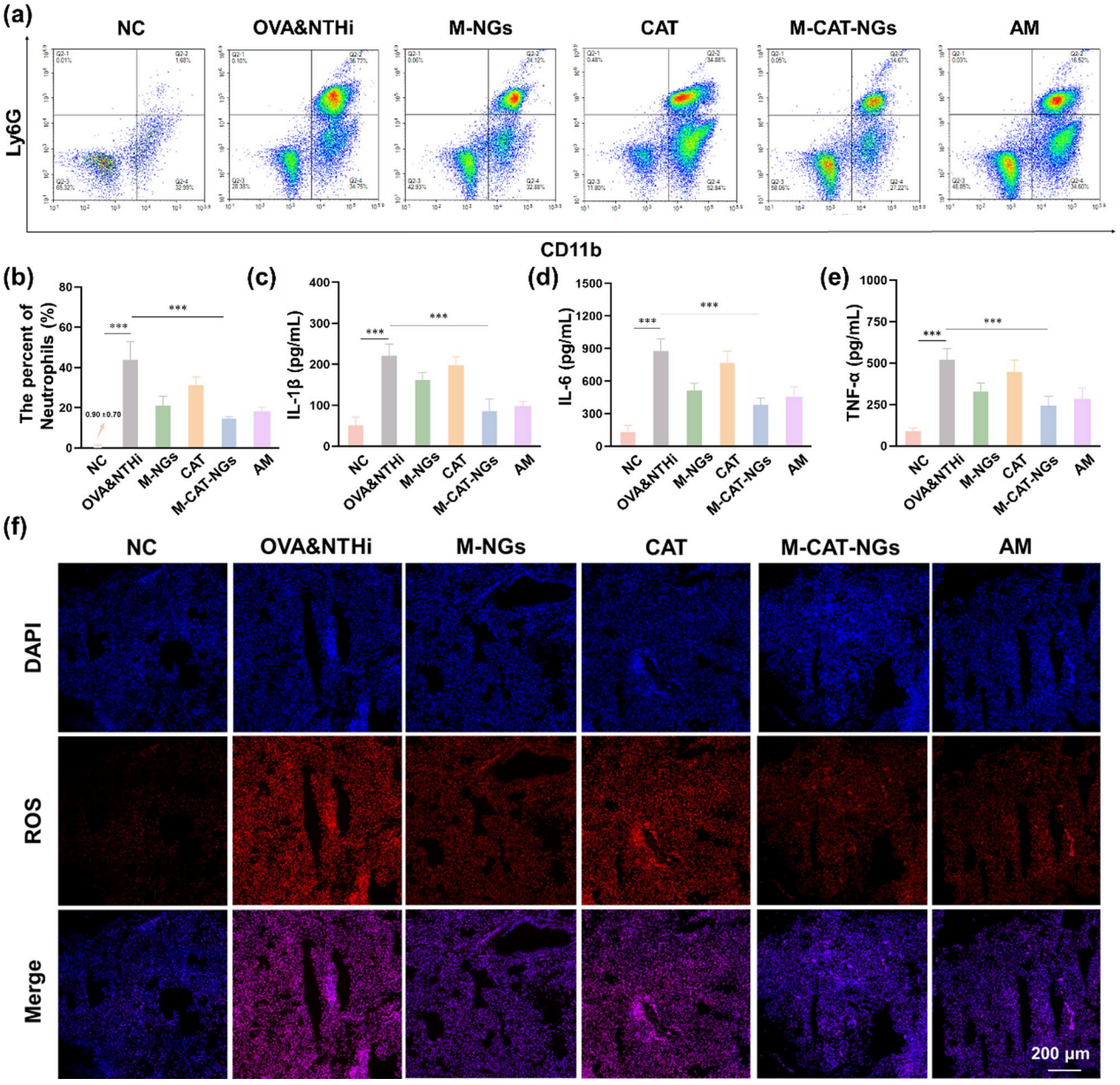

Fig. 5 (**a**) Flow cytometric analysis of neutrophils ($CD11b^+/Ly6G^+$) present in BALF. (**b**) The count of the percentage of neutrophils in (**a**) ($n=6$). (**c**-**e**) Expressions of IL-1β, IL-6 and TNF-α in lung after different sample treatments ($n=6$), (**f**) ROS expression in lung tissues after different treatments. The scale bar represented 200 μm, $^{***}p<0.001$

the proportion of neutrophils in BALF of neutrophilic asthma mice probably due to their excellent antibacterial ability and the CAT in M-CAT-NGs could eliminate ROS. There was no significant change in the proportion of neutrophils in the CAT group compared to the OVA&NTHi group might be due to the CAT shows no antimicrobial ability and native CAT is not stable enough and easily broken down *in vivo*. Besides, IL-1β, IL-6 and TNF-α associated with asthma were tested and obtained similar results (Fig. 5c-e). OVA and NTHi treatment could induce the expression of inflammatory cytokines and produce an inflammatory response. The expressions of IL-1β, IL-6 and TNF-α were not reduced after treatment with CAT but those were significantly decreased after M-NGs, M-CAT-NGs and AM treatments. It was noteworthy that the expressions of IL-1β, IL-6 and TNF-α showed the most significant reduction after treatment with M-CAT-NGs. In addition, ROS aggregation and its mediated oxidative stress damage played an important role in asthma [28]. To investigate whether M-CAT-NGs could mitigate the accumulation of ROS in lung, the expression level of ROS in lung tissues was

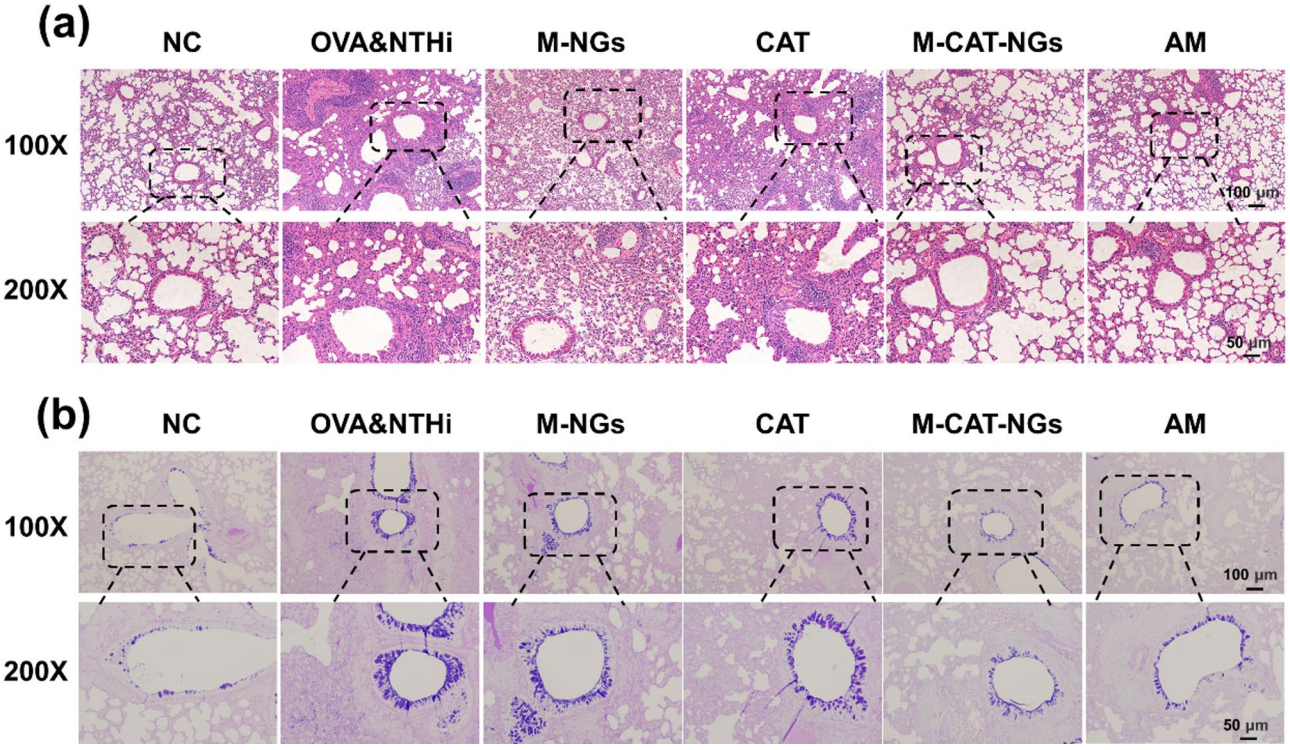

Fig. 6 (**a**) Histological examination of the lungs of mice in each group by H&E staining. (**b**) Bronchial AB-PAS staining images of lung tissues in each group of mice. The scale bars indicated 100 μm and 50 μm, respectively

measured. As shown in Fig. 5f, the level of ROS production in lung tissues was significantly increased after OVA&NTHi treatment compared with NC group. Compared with the OVA&NTHi group, M-NGs, M-CAT-NGs and AM treatment led to a decrease in ROS levels in lung tissue, among which the reduction was most significant after M-CAT-NGs treatment. There was no significant change in the CAT group, indicating that M-NGs and AM might reduce the production of ROS in lung tissue through their antibacterial effects, while M-CAT-NGs could exert therapeutic effects from two perspectives: antibacterial activity and encapsulation of CAT to form nanogels, thereby enhancing CAT solubility and improving its bioavailability. The above results suggested that M-CAT-NGs could regulate inflammatory responses *in vivo* and potentially treat neutrophilic asthma.

Morphologic changes in lung tissue

Pathologically, the main features of asthma included chronic inflammation, airway tissue remodeling, disruption of epithelial integrity [56], cupped cell hyperplasia [57, 58], and dysregulation of mucus secretion [49]. To investigate whether M-CAT-NGs could ameliorate pathological changes in lung tissue, lung tissues from mice were stained with H&E and observed. As illustrated in Fig. 6a and Fig. S21, the OVA&NHTi group exhibited pronounced thickening of the bronchioles and alveolar septa when compared to the NC group, increased alveolar fusion. No significant improvement in the bronchi and alveoli was observed after CAT treatment. M-NGs and M-CAT-NGs groups showed attenuated bronchiolar thickening in the lung tissues, with the alveolar septa relatively intact, and a significant reduction in the number of inflammatory cell infiltrates. This might be due to both M-NGs and M-CAT-NGs had good antimicrobial capacity, especially M-CAT-NGs also increased the bioavailability of CAT and promoted the uptake of M-CAT-NGs by the epithelial cells, which reduced the effect of bacterial infections on the integrity of the alveolar-capillary barrier and moderated inflammatory responses and reduced the infiltration of inflammatory cells [59].

Studies have shown that infection with NTHi in asthma patients leads to goblet cells proliferation, upregulation of the mucin MUC5AC [60], and airway mucus became more abundant and viscous, resulting in ciliary dysfunction, coupled with mucus embolism and compromised mucosal ciliary clearance [61]. Bronchial stasis impaired pathogen clearance, thereby facilitating the colonization of NTHi. Consequently, NTHi robustly induced the transcription of MUC5AC via the upregulation of the MAPK pathway, while also enhancing the expression of the highly insoluble MUC2 mucin through NF-κB and TGF-β/Smad signaling [62]. Diffuse mucus occlusion of the airways could lead to localized atelectasis, which

could worsen symptoms in patients with asthma and greatly increase asthma mortality [63]. Consequently, alleviating mucus secretion within the airways is crucial for the effective management of asthma. The results of AB-PAS staining showed significantly higher levels of airway mucus secretion in the OVA&NTHi group compared with the NC group, indicating that sensitization with OVA, coupled with NTHi infection, markedly elevated mucus secretion levels within the airways of the mice (Fig. 6b and Fig. S22). Compared with the OVA&NHTi group, the M-CAT-NGs group showed a significant decrease in mucus, which might be attributed to the fact that M-CAT-NGs inhibited bacterial colonization within the mucus layer, contributing to an enhanced mucus environment, leading to a decrease in mucus. Similarly, mucus in the airways of mice was also significantly reduced after nebulization with M-NGs compared to the OVA&NTHi group whereas no significant change in mucus was observed in the CAT group, which might be attributed to the excellent antimicrobial capacity of M-NGs and M-CAT-NGs, which inhibited the growth of NTHi, thus alleviating mucus obstruction in the airway. To detect the longer-term therapeutic effect after medication, we conducted lung function tests and pathological section examinations on mice on the 14th and 31st days after the cessation of M-CAT-NGs treatment. As shown in Fig. S23, M-CAT-NGs-treated mice exhibited comparable respiratory parameters to NC controls. H&E and AB-PAS staining revealed resolution of in treated mice at both timepoints, with no rebound pathology (Fig. S24).

H&E staining observations and blood biochemical indicator tests were conducted to investigate whether the structure and function of major organs in mice would be damaged by M-CAT-NGs. As depicted in Fig. S25, treatment with 0.96 mg/mL of M-NGs, CAT, and M-CAT-NGs did not result in any significant alterations to the organ tissue structure when compared to the NC group. Specifically, no pathological alterations were observed in the myocardial striations, and the fundamental structural components of the liver-namely, the central vein, hepatic sinusoids, and bile ducts-exhibited clear structural integrity. The splenic capsule and trabeculae, white and red medulla, and parenchymal marginal regions were also structurally intact. The interstitium and parenchyma of the lungs were well defined. The glomeruli and tubules of the kidneys also did not show any pathologic changes. Similar results were obtained in the blood biochemical indices, and there were no significant changes in all indices such as alanine aminotransferase (ALT), aspartate aminotransferase (AST), alkaline phosphatase (AKP), uric acid (UA), blood urea nitrogen (BUN) and creatinine (CRE) in all groups of mice compared with the control group (Fig. S26), which indicated that M-NGs, CAT and M-CAT-NGs had no significant effect on the hepatic and renal functions of mice. In conclusion, M-NGs, CAT, and M-CAT-NGs showed no significant toxicity to mice, either in terms of morphology or liver and kidney functions, providing strong evidence of safety *in vivo*.

The *in vivo* results demonstrated that M-CAT-NGs exhibited significant therapeutic effects in OVA&NTHi-induced neutrophilic asthma mice, which were mainly reflected in the ability of M-CAT-NGs to significantly improve the lung function of neutrophilic asthma mice, reduce the proportion of neutrophilic cells, decrease the mucus secretion of the airways, restore the normal morphology of the airways, clean ROS from the lungs, and alleviate inflammation in the lungs. The therapeutic effects of M-NGs were similar to those of M-CAT-NGs, but M-NGs exhibited no significant role in cleaning ROS *in vivo*. This might be due to M-NGs did not contain the key component, i.e. CAT, for decomposing ROS. Although free-form CAT showed good efficiency in decomposition of H_2O_2*in vitro*, it did not show therapeutic effects in neutrophilic asthma mice *in vivo*. This result might be due to free CAT was unstable and susceptible to destruction and loss of bioactivity.

Conclusion

In this study, we successfully synthesized a kind of multifunctional nanogels (M-CAT-NGs) through ionic crosslinking and chemical conjugation. The obtained M-CAT-NGs possessed excellent antimicrobial ability and were able to release CAT responsively in the presence of MMP-9. *In vitro* experiments confirmed that M-CAT-NGs had excellent anti-inflammatory abilities, which could reduce H_2O_2-induced ROS production and down-regulate LPS-induced expression of IL-1β, IL-6, and TNF-α. *In vivo* experiments showed that M-CAT-NGs could effectively accumulate in the lungs, and the treatment with M-CAT-NGs significantly improved AHR, inhibited neutrophil accumulation in the lungs, reduced ROS levels in lung tissues, relieved airway mucus obstruction, and attenuated airway inflammation by regulating inflammatory responses. In conclusion, the CAT-loaded MMP-9-responsive nanogels achieved encouraging therapeutic effects in OVA&NTHi-induced neutrophilic asthma mice, and showed great potential in terms of antimicrobial, anti-inflammatory, and therapeutic efficacy in treating neutrophilic asthma.

Supplementary Information

The online version contains supplementary material available at https://doi.org/10.1186/s12951-025-03470-3.

Supplementary Material 1

Acknowledgements
Not applicable.

Author contributions
X.G., F.W., C.X., and C.H. designed the experiments, performed data analysis, and wrote the main manuscript. X.G., X.Z., W.Z. performed most of the experiments. X.G., F.W., C.X. and D.Z. discussed the data and their interpretation. C.D., Z.Z., and Y.S. provided technical support. F.W., C.X., and C.H. were the providers of the program funds. All authors read and approved the final manuscript.

Funding
The authors are thankful to the supports from the National Key Research & Development Program of China (2022YFC2604000), the National Natural Science Foundation of China (52073278), the "Medical Science + X" Cross-innovation Team of the Norman Bethune Health Science of Jilin University (2022JBGS10), Key Laboratory of Precision Infectious Diseases of Jilin Province (20200601011JC), and Jilin Provincial Key Laboratory of Pathogen Biology International Science, Technology Cooperation (20230502002GH), Jilin province science and technology development program (20230101045JC) and Education Department of Jilin Province (JJKH20231205KJ).

Data availability
No datasets were generated or analysed during the current study.

Declarations

Ethics approval and consent to participate
All animal experimental protocols were approved by the Animal Care and Use Review Committee of Jilin University and received approval from the Animal Ethics Committee of the College of Basic Medical Sciences at Jilin University (No. 2023 – 444).

Consent for publication
All authors of this study agreed to publish.

Competing interests
The authors declare no competing interests.

Received: 3 April 2025 / Accepted: 16 May 2025
Published online: 24 May 2025

References

1. Hammad H, Lambrecht BN. The basic immunology of asthma. Cell. 2021;184(6):1469–85.
2. Pavord ID, et al. After asthma: redefining airways diseases. Lancet. 2018;391(10118):350–400.
3. Hopkin JM. The diagnosis of asthma, a clinical syndrome. Thorax. 2012;67(7):660–2.
4. Papi A, et al. Asthma Lancet. 2018;391(10122):783–800.
5. Ortega HG, et al. Severe eosinophilic asthma treated with mepolizumab stratified by baseline eosinophil thresholds: a secondary analysis of the DREAM and MENSA studies. Lancet Respir Med. 2016;4(7):549–56.
6. Agache I, et al. Advances and highlights in asthma in 2021. Allergy. 2021;76(11):3390–407.
7. Chung KF, et al. International ERS/ATS guidelines on definition, evaluation and treatment of severe asthma. Eur Respir J. 2014;43(2):343–73.
8. Grunwell JR, et al. Children with neutrophil-predominant severe asthma have Proinflammatory neutrophils with enhanced survival and impaired clearance. J Allergy Clin Immunol Pract. 2019;7(2):516–e5256.
9. Zhang J, et al. The role of NTHi colonization and infection in the pathogenesis of neutrophilic asthma. Respir Res. 2020;21(1):170.
10. Ordonez CL, et al. Increased neutrophil numbers and IL-8 levels in airway secretions in acute severe asthma: clinical and biologic significance. Am J Respir Crit Care Med. 2000;161(4 Pt 1):1185–90.
11. Moore WC, et al. Sputum neutrophil counts are associated with more severe asthma phenotypes using cluster analysis. J Allergy Clin Immunol. 2014;133(6):1557–e635.
12. Huang YJ, et al. The airway Microbiome in patients with severe asthma: associations with disease features and severity. J Allergy Clin Immunol. 2015;136(4):874–84.
13. Bisgaard H, et al. Childhood asthma after bacterial colonization of the airway in neonates. N Engl J Med. 2007;357(15):1487–95.
14. Wood LG, et al. Potentially pathogenic bacteria cultured from the sputum of stable asthmatics are associated with increased 8-isoprostane and airway neutrophilia. Free Radic Res. 2010;44(2):146–54.
15. Simpson JL, et al. Airway dysbiosis: Haemophilus influenzae and Tropheryma in poorly controlled asthma. Eur Respir J. 2016;47(3):792–800.
16. Green BJ, et al. Potentially pathogenic airway bacteria and neutrophilic inflammation in treatment resistant severe asthma. PLoS ONE. 2014;9(6):e100645.
17. Tchoupa AK, et al. Outer membrane protein P1 is the CEACAM-binding adhesin of Haemophilus influenzae. Mol Microbiol. 2015;98(3):440–55.
18. Kenjale R, et al. Structural determinants of autoproteolysis of the Haemophilus influenzae hap autotransporter. Infect Immun. 2009;77(11):4704–13.
19. Weiser JN, Pan N. Adaptation of Haemophilus influenzae to acquired and innate humoral immunity based on phase variation of lipopolysaccharide. Mol Microbiol. 1998;30(4):767–75.
20. King PT, et al. Nontypeable Haemophilus influenzae induces sustained lung oxidative stress and protease expression. PLoS ONE. 2015;10(3):e0120371.
21. Ranneh Y, et al. Crosstalk between reactive oxygen species and pro-inflammatory markers in developing various chronic diseases: a review. Appl Biol Chem. 2017;60(3):327–38.
22. Atkinson JJ, Senior RM. Matrix metalloproteinase-9 in lung remodeling. Am J Respir Cell Mol Biol. 2003;28(1):12–24.
23. Song Y, et al. miR-181-5p attenuates neutrophilic inflammation in asthma by targeting DEK. Int Immunopharmacol. 2022;112:109243.
24. Lee SJ et al. Protective effects of Angelica decursiva Franchet & Savatier on allergic responses through enhancement of Nrf2 and suppression of NF-kB/MMP-9 in ovalbumin-exposed mice. J Ethnopharmacol. 2024;318(Pt A):116863.
25. Andreadis AA, et al. Oxidative and nitrosative events in asthma. Free Radic Biol Med. 2003;35(3):213–25.
26. Schieber M, Chandel NS. ROS function in redox signaling and oxidative stress. Curr Biol. 2014;24(10):R453–62.
27. Sies H, Jones DP. Reactive oxygen species (ROS) as pleiotropic physiological signalling agents. Nat Rev Mol Cell Biol. 2020;21(7):363–83.
28. Michaeloudes C, et al. Molecular mechanisms of oxidative stress in asthma. Mol Aspects Med. 2022;85:101026.
29. Nishikawa M, Hashida M, Takakura Y. Catalase delivery for inhibiting ROS-mediated tissue injury and tumor metastasis. Adv Drug Deliv Rev. 2009;61(4):319–26.
30. Qin M, et al. An antioxidant enzyme therapeutic for COVID-19. Adv Mater. 2020;32(43):e2004901.
31. Islam N, Ferro V. Recent advances in chitosan-based nanoparticulate pulmonary drug delivery. Nanoscale. 2016;8(30):14341–58.
32. Deslouches B, et al. Comparative functional properties of engineered cationic antimicrobial peptides consisting exclusively of Tryptophan and either lysine or arginine. J Med Microbiol. 2016;65(6):554–65.
33. Wang L, et al. Epsilon-poly-l-lysine: recent advances in biomanufacturing and applications. Front Bioeng Biotechnol. 2021;9:748976.
34. Alfonso-Prieto M, et al. The molecular mechanism of the catalase reaction. J Am Chem Soc. 2009;131(33):11751–61.
35. Lueckgen A, et al. Enzymatically-degradable alginate hydrogels promote cell spreading and in vivo tissue infiltration. Biomaterials. 2019;217:119294.
36. Hsu AC, et al. Targeting PI3K-p110alpha suppresses influenza virus infection in chronic obstructive pulmonary disease. Am J Respir Crit Care Med. 2015;191(9):1012–23.
37. Guan X, et al. The role of regulatory T cell in nontypeable Haemophilus influenzae-induced acute exacerbation of chronic obstructive pulmonary disease. Mediators Inflamm. 2018;2018:p8387150.
38. Zhang P, et al. Charge reversal nano-systems for tumor therapy. J Nanobiotechnol. 2022;20(1):31.
39. Uzhytchak M, et al. Lysosomal nanotoxicity: impact of nanomedicines on lysosomal function. Adv Drug Deliv Rev. 2023;197:114828.
40. Zhou J, et al. Cellular uptake of a taurine-modified, ester bond-decorated D-peptide derivative via dynamin-based endocytosis and macropinocytosis. Mol Ther. 2018;26(2):648–58.
41. Sies H. Hydrogen peroxide as a central redox signaling molecule in physiological oxidative stress: oxidative eustress. Redox Biol. 2017;11:613–9.

42. Han M, et al. Toll-like receptor 2-expressing macrophages are required and sufficient for rhinovirus-induced airway inflammation. J Allergy Clin Immunol. 2016;138(6):1619–30.
43. Beigelman A, et al. Randomized trial to evaluate Azithromycin's effects on serum and upper airway IL-8 levels and recurrent wheezing in infants with respiratory syncytial virus bronchiolitis. J Allergy Clin Immunol. 2015;135(5):1171–e81.
44. Wang G, et al. Combined treatment with SB203580 and dexamethasone suppresses non-typeable Haemophilus influenzae-induced Th17 inflammation response in murine allergic asthma. Eur J Pharmacol. 2019;862:172623.
45. Tillie-Leblond I, et al. Relation between inflammation and symptoms in asthma. Allergy. 2009;64(3):354–67.
46. Sly PD, et al. Early identification of atopy in the prediction of persistent asthma in children. Lancet. 2008;372(9643):1100–6.
47. Holt PG, Sly PD. Viral infections and atopy in asthma pathogenesis: new rationales for asthma prevention and treatment. Nat Med. 2012;18(5):726–35.
48. Holtzman MJ. Asthma as a chronic disease of the innate and adaptive immune systems responding to viruses and allergens. J Clin Invest. 2012;122(8):2741–8.
49. Ackland J, et al. Nontypeable Haemophilus influenzae infection of pulmonary macrophages drives neutrophilic inflammation in severe asthma. Allergy. 2022;77(10):2961–73.
50. Rashki S, et al. Chitosan-based nanoparticles against bacterial infections. Carbohydr Polym. 2021;251:117108.
51. Liu F, et al. Preparation and antibacterial properties of epsilon-polylysine-containing Gelatin/chitosan nanofiber films. Int J Biol Macromol. 2020;164:3376–87.
52. Antunes BP, et al. Chitosan/arginine-chitosan polymer blends for assembly of nanofibrous membranes for wound regeneration. Carbohydr Polym. 2015;130:104–12.
53. Lu J, et al. The role of lower airway dysbiosis in asthma: dysbiosis and asthma. Mediators Inflamm. 2017;2017:p3890601.
54. Brusasco V, Crimi E. Methacholine provocation test for diagnosis of allergic respiratory diseases. Allergy. 2001;56(12):1114–20.
55. Busse WW. The relationship of airway hyperresponsiveness and airway inflammation: airway hyperresponsiveness in asthma: its measurement and clinical significance. Chest. 2010;138(2 Suppl):S4–10.
56. Bousquet J, et al. Asthma. From bronchoconstriction to airways inflammation and remodeling. Am J Respir Crit Care Med. 2000;161(5):1720–45.
57. Benayoun L, et al. Airway structural alterations selectively associated with severe asthma. Am J Respir Crit Care Med. 2003;167(10):1360–8.
58. Carroll NG, Mutavdzic S, James AL. Increased mast cells and neutrophils in submucosal mucous glands and mucus plugging in patients with asthma. Thorax. 2002;57(8):677–82.
59. Lucas R, et al. Impact of bacterial toxins in the lungs. Toxins (Basel). 2020;12(4):223.
60. Aikawa T, et al. Marked goblet cell hyperplasia with mucus accumulation in the airways of patients who died of severe acute asthma attack. Chest. 1992;101(4):916–21.
61. Panchabhai TS, et al. Plugs of the air passages: a clinicopathologic review. Chest. 2016;150(5):1141–57.
62. Brown MA et al. Non-typeable Haemophilus influenzae airways infection: the next treatable trait in asthma? Eur Respir Rev, 2022. 31(165).
63. Fahy JV, Dickey BF. Airway mucus function and dysfunction. N Engl J Med. 2010;363(23):2233–47.

Publisher's note